Journal of Power Sources 195 (2010) 367–373

Contents lists available at ScienceDirect

Journal of Power Sources

journal homepage: www.elsevier.com/locate/jpowsour

Structure, morphology and electrochemical behaviour of manganese oxides prepared by controlled decomposition of permanganate

S.W. Donne[a], A.F. Hollenkamp[b,*], B.C. Jones[a]

[a] Discipline of Chemistry, University of Newcastle, Callaghan, NSW 2308, Australia
[b] CSIRO Energy Technology, Box 312, Clayton South, Vic. 3169, Australia

ARTICLE INFO

Article history:
Received 27 May 2009
Accepted 17 June 2009
Available online 10 July 2009

Keywords:
Manganese dioxide
Birnessite
Supercapacitor
Composite electrode
Pseudo-capacitance

ABSTRACT

Hydrothermal decomposition of permanganate, conducted in a range of pH-controlled solutions (from strongly acidic to strongly basic), is used to prepare manganese dioxides that are well-suited for use as supercapacitor electrode materials. While permanganate is thermodynamically unstable, the kinetics of its decomposition in an aqueous environment are very slow, until the temperature is raised to ~200 °C. Although the resultant materials are relatively crystalline and have low total pore volume, their prominent meso-porosity leads to good electrochemical performance. Best behaviour is obtained for material from permanganate decomposition in 0.01 M H_2SO_4 solution, for which composite electrodes (150 μm thick) yield ~150 F g^{-1} at 5 mV s^{-1} in a 9 M KOH electrolyte.

1. Introduction

Modern society is very dependent on electrical energy that most often is generated from power stations burning fossil fuels (coal, oil and natural gas). Of course these are unfortunately major contributors to environmental greenhouse gas emissions. Many other sources of energy exist (*e.g.*, nuclear, hydroelectric, solar, geothermal, wind, biomass), but none is a realistic and economic substitute for fossil-fuel-based power [1]. Therefore, energy production in the future is anticipated to be more distributed in nature in that it will capitalize on combinations of smaller-scale alternative forms of energy.

With the future of energy production heading in such a direction, there will be an increase in the importance of energy storage as a means to provide load-levelling capabilities. Batteries, supercapacitors and fuel cells are well-known options, in which case the energy is stored chemically. The relative merits of these three types of electrochemical cell can be summarized by a Ragone diagram [2] which shows that fuel cells provide the highest specific energy, but at quite low specific power, while the performance of supercapacitors is essentially the converse. Batteries generally occupy an intermediate region within the Ragone plot they provide higher specific energy than supercapacitors and greater specific power than fuel cells. Globally, research continues with the aim of increasing the performance of these storage media, as well as identifying optimum applications.

The objective basis of this research project is to improve the performance of supercapacitor electrodes by raising their specific energy, thus making them more broadly applicable as power sources. Commercially supercapacitors are symmetrical devices that employ activated carbon electrodes with either an aqueous (*e.g.*, H_2SO_4) or a non-aqueous (*e.g.*, tetra alkyl ammonium tetrafluoroborate in acetonitrile) based electrolyte [3]. The performance of these devices is quite good (high specific power and long cycle-life) yet, as mentioned above, their specific energy is very limited. An approach to improving specific energy is to incorporate a pseudo-capacitive electrode [4], *i.e.*, an electrode that can store charge in the double-layer, as a conventional supercapacitor electrode would do, as well as undergo fast and reversible surface redox reactions (faradaic reactions). The latter feature provides enhanced specific capacitance (in F g^{-1}), compared with carbon-based electrodes, because the chemical storage of a redox-based electrode embodies substantially greater charge density than the electrostatic storage of simple double-layer electrodes.

The archetypal material for pseudo-capacitive electrodes is amorphous hydrated ruthenium dioxide ($RuO_2 \cdot xH_2O$) which has been reported to have a capacitance approaching 900 F g^{-1} in an aqueous H_2SO_4 electrolyte [5]. With cost limiting the commercial implementation of this ruthenium-based electrode, the search for suitable alternatives has considered other metal oxides and also conductive polymers. Of these, metal oxides are preferred because of their higher density [4,5], with systems based on manganese dioxide presently receiving considerable attention [6]. This

* Corresponding author. Tel.: +61 3 9545 8903; fax: +61 3 9562 8919.
E-mail address: Tony.Hollenkamp@csiro.au (A.F. Hollenkamp).

0378-7753/$ – see front matter.
doi:10.1016/j.jpowsour.2009.06.103

is mainly because numerous methods of synthesis [7] provide exceptional control over product morphology which, when coupled with good faradaic electrochemical performance, low cost and environmental friendliness, means that this class of materials is a strong candidate for application in the next generation of supercapacitor devices. This study reports the synthesis, characterization and performance of manganese dioxides that are formed from the spontaneous decomposition of permanganate in a range of different aqueous electrolytes at different temperatures.

2. Experimental

2.1. Sample preparation

Manganese dioxide samples were prepared via the spontaneous decomposition of permanganate (either Na or K salts; Sigma–Aldrich) under hydrothermal conditions in an acid digestion bomb (Parr Instrument Company, volume = 23 ml). In the Teflon cup of the bomb, permanganate salt (0.0115 mole) was weighed, followed by 15 ml of electrolyte and gentle agitation to facilitate dissolution. The electrolytes examined for their effects on the decomposition of permanganate ranged from strongly acidic (1 M H_2SO_4) to strongly basic (1 M NaOH or KOH). After dissolution of the permanganate, the digestion bomb was sealed and placed in an oven (reaction temperature set from ambient up to 200 °C) where it was left for a period of 5 days. The vessel was then removed from the oven and allowed to cool to room temperature. Any solids formed were collected by filtration, and subjected to a washing sequence designed to retain the pore structure in the solid by minimizing the surface tension at the solid–liquid interface when drying takes place [8]. The first stage of the procedure was to wash the solid thoroughly on the filter paper with Milli Q ultra-pure water (surface tension of 72.75 mN m^{-1} at 20 °C) until the filtrate had the same pH as the wash water. The solid was then re-suspended in acetone (surface tension of 23.70 mN m^{-1} at 20 °C [9]) for 1 h to extract water from the pores. The suspension was then filtered, and the re-suspension process repeated this time with liquid hexane (surface tension of 18.43 mN m^{-1} at 20 °C). After this third washing the suspension was filtered and then dried in air at 50 °C.

2.2. Physical and morphological characterization

The material structure was examined by means of X-ray diffraction with a Philips 1710 diffractometer equipped with a Cu Kα radiation source (λ = 1.5418 Å) and operated at 40 kV and 30 mA. The scan range was from 10 to 90°2θ, with a step size of 0.1° and a count time of 2.5 s.

Morphology was examined in a Philips XL30 scanning electron microscope (SEM) at a range of magnifications. Surface area and porosity were quantified by gas adsorption with a Micromeritics ASAP 2020 Analyzer; the samples were degassed under vacuum at 110 °C prior to analysis using N_2 as the adsorbate at 77 K. The specific surface area was extracted from the gas adsorption data using the BET isotherm [10], while the pore-size distribution was determined by means of an approach based on Density Functional Theory (Micromeritics DFTPlus V2.00) [11].

2.3. Electrode preparation

Electrodes were prepared from a 10:1 mixture of Timcal SFG6 graphite and the manganese dioxide sample (referred to as a 'blackmix'), which was moistened to form a paste by the addition of an extra 10 wt.% of electrolyte (9 M KOH). Once made, the blackmix was stored in an airtight container for at least 24 h to ensure adequate penetration of the electrolyte into the manganese dioxide pores. An amount of blackmix corresponding to 10 mg of manganese dioxide was then placed into the base of a Teflon-lined, gold-coated, stainless-steel cup (13 mm radius), which was covered with two layers of separator paper, and then compacted under a pressure of 1 t (for 1 min). The resulting composite electrode had a thickness of ~150 μm and was then covered by a perforated Perspex disc with a stainless-steel sleeve inserted into cell to retain the disc in place and also function as a counter electrode. The components of the complete test cell are shown schematically in Fig. 1. The cell assembly was held together by a frame that consisted of a base- and cover-plate connected by three securing

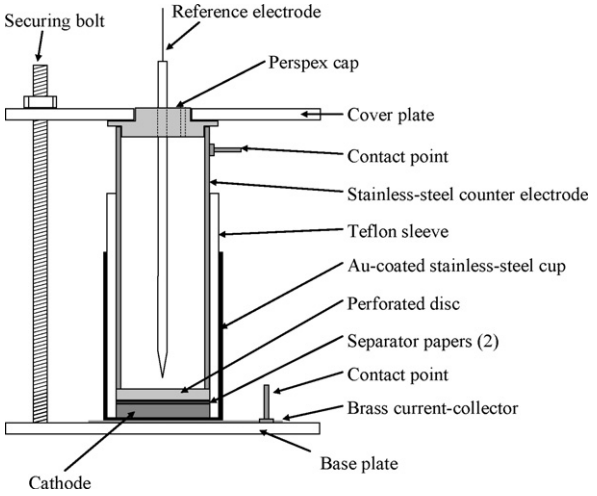

Fig. 1. Schematic diagram of electrochemical cell.

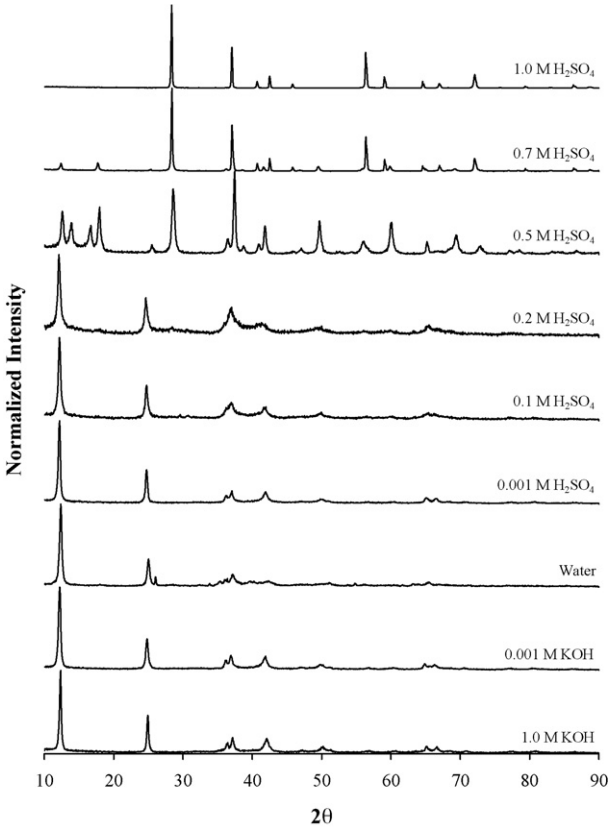

Fig. 2. Selected XRD patterns for hydrothermally prepared (200 °C) manganese dioxide.

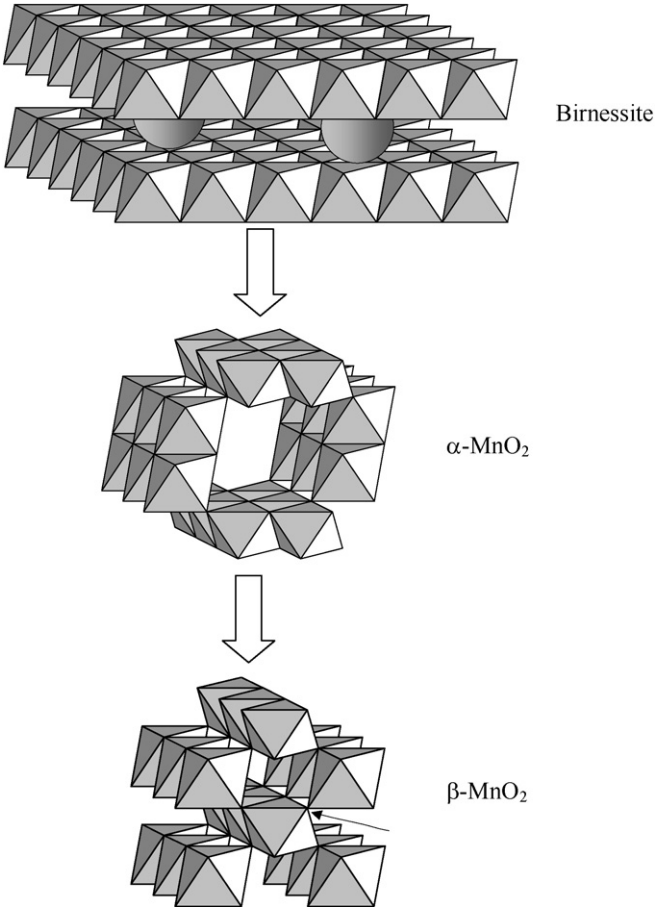

Fig. 3. Manganese dioxide structural transitions induced during material synthesis.

bolts, which were tightened to a torque of 0.75 Nm to ensure a uniform pressure on the electrode during electrochemical cycling. Approximately 10 ml of electrolyte (9 M KOH) was added to the cell, together with a Hg/HgO reference electrode. All potentials are reported with respect to this reference electrode. The cell in this state was allowed to rest for 1 h before electrochemical cycling to ensure adequate penetration of the electrolyte into the electrode.

2.4. Electrochemical protocol

The performance of the electrode materials was evaluated by means of cyclic voltammetry at scan rates of 5, 25 and 50 mV s^{-1} for at least 100 cycles, over a voltage window from +0.4 to −0.4 V. The experiments were conducted with an EG&G Princeton Applied Research M362 Scanning Potentiostat. Data acquisition was controlled with LabView software.

3. Results and discussion

3.1. Synthesis experiments

During the initial experiments, it became apparent that the 5-day period allowed for permanganate decomposition was not sufficient, except at the highest temperature used, *i.e.*, 200 °C. In fact, extended heating of the permanganate, in some instances for up to 2–3 weeks, did not yield sufficient product for characterization, even at a temperature of 160 °C. From that point, all materials were produced at 200 °C.

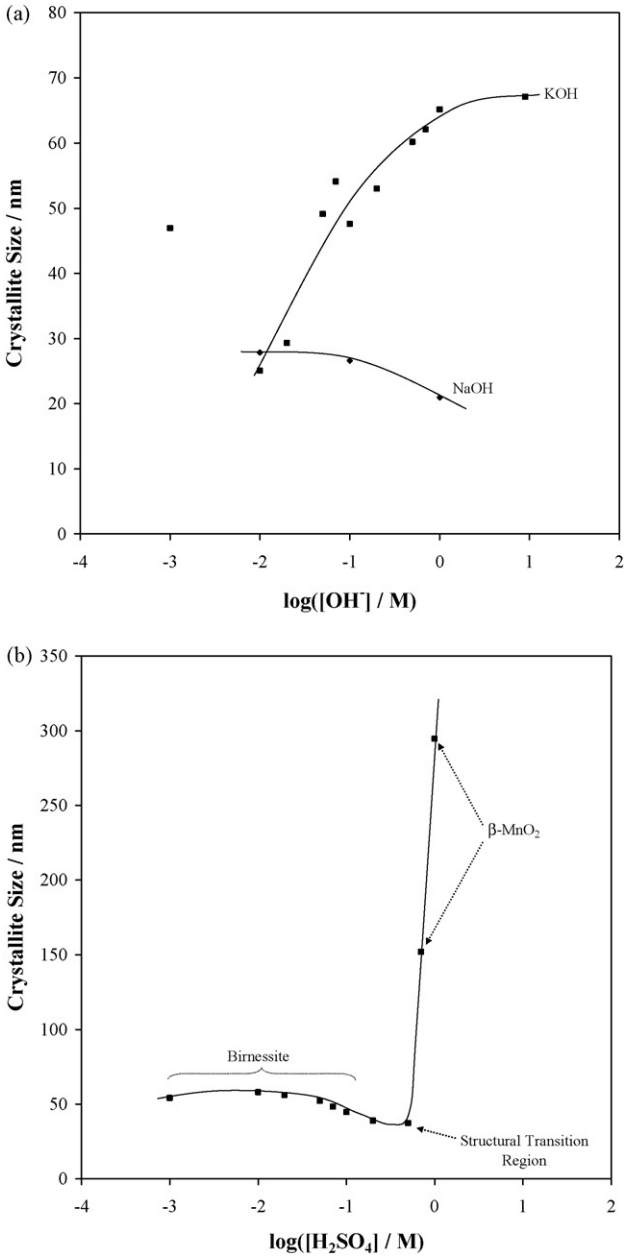

Fig. 4. Crystallite dimensions as function of (a) OH^- and (b) H_2SO_4 concentrations used during manganese dioxide synthesis. Note that birnessite is the only phase produced in the base synthesis.

3.2. Material structure

A selection of X-ray diffraction patterns, for materials produced under a range of solution conditions, is presented in Fig. 2. Essentially, the manganese dioxide phase birnessite is produced when using basic conditions and H_2SO_4 acid concentrations up to 0.2 M, irrespective of whether $NaMnO_4$ or $KMnO_4$ is used as the starting material. Birnessite has a layered structure [12], in which any foreign metal ions or water reside in the interlayer region (Fig. 3). Crystallographically, birnessite has been reported to have a wide range of symmetries that include hexagonal (a_0 = 5.82 Å and c_0 = 14.62 Å [13], a_0 = 2.84 Å and c_0 = 7.27 Å [14]), orthorhombic (a_0 = 8.54 Å, b_0 = 15.39 Å and c_0 = 14.26 Å [15]) and monoclinic (a_0 = 5.149 Å, b_0 = 2.843 Å, c_0 = 7.176 Å and β = 100.76° [16]), This range is a reflection of the level of disorder that can be induced in the structure. When 0.5 M H_2SO_4 is used, a mixture of phases

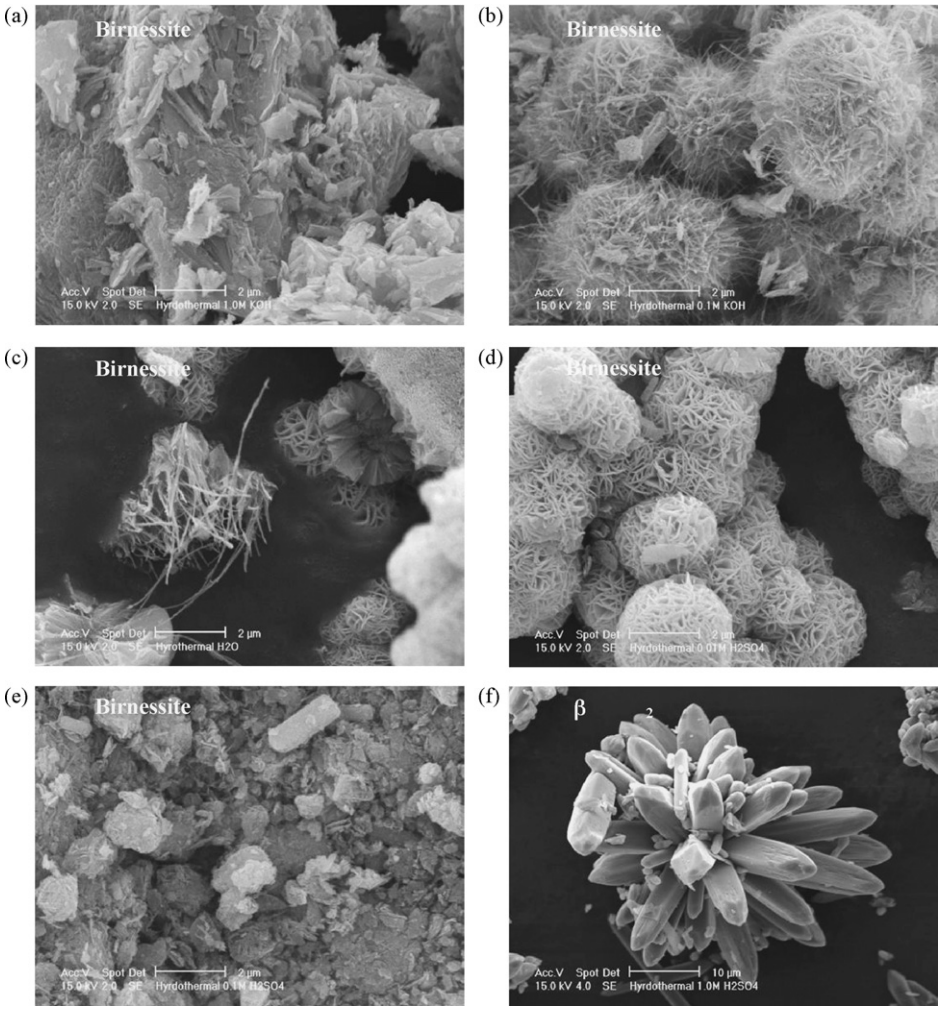

Fig. 5. SEM images of selected manganese dioxide samples produced by decomposition of permanagante in different electrolytes, (a) 1 M KOH, (b) 0.1 M KOH, (c) water, (d) 0.01 M H_2SO_4, (e) 0.1 M H_2SO_4, and (f) 1.0 M H_2SO_4. Predominant structure is indicated in each micrograph.

is produced, which includes α-MnO_2 and β-MnO_2, whereas in ≥0.7 M H_2SO_4, β-MnO_2 is the preferred phase (Fig. 3). Both α- and β-MnO_2 have tunnel structures [12] (2 × 2 octahedral units for α-MnO_2, and 1 × 1 octahedral units for β-MnO_2). Both have also been reported to possess tetragonal symmetry (a_0 = 9.84 Å and c_0 = 2.86 Å for α-MnO_2 [12], and a_0 = 4.39 Å and c_0 = 2.87 Å for β-MnO_2 [12]). Whether NaOH or KOH is used as the basic electrolyte, birnessite is still the manganese dioxide phase produced.

Clearly birnessite is the preferred product under all but the most acidic solution conditions. Comparing the general features of the structural forms shown in Fig. 3, the effect of increasingly acidic conditions is a progression from the relatively open, layered structure of birnessite, through the relatively large tunnel structured phase α-MnO_2, to the more compact and dense β-MnO_2 phase. Birnessite derives its structural stability from the presence of foreign metal ions (*e.g.*, K^+, Na^+, in the present case) between the layers of MnO_6 octahedra, since without these species the structure collapses to a tunnel structure [12]. As is apparent in this work, the extent of the structural transition is also sensitive to the molar ratio of foreign metals to protons ($n(M^+)$:$n(H^+)$), for which there appears to be a critical value for tunnel structure formation. Indeed, the tunnel structure first forms in 0.5 M H_2SO_4 electrolyte, *i.e.*, the first composition in which the $n(M^+)$:$n(H^+)$ ratio falls below 1 (0.77 in this case). This indicates that during synthesis there is competition between the foreign metal ions and protons for the same sites in the newly formed manganese dioxide structure. When suitable foreign metal ions are in excess, a templating effect predominates to form birnessite. When protons are in excess, however, the structure collapses to form tunnels. While this conclusion applies for samples synthesized at 200 °C, the critical $n(M^+)$:$n(H^+)$ ratio may be different at other temperatures.

The crystallinity of each manganese dioxide sample was also extracted from the XRD patterns using the Scherrer equation [17]; the results are shown in Fig. 4(a) and (b). First, when KOH is used as the electrolyte, the data indicate that sample crystallinity (as indicated by average crystal size from the Scherrer analysis) increases with KOH concentration (Fig. 4(a)). This points to the conclusion that K^+ is a good templating cation for the birnessite structure. By contrast, an increase in NaOH concentration causes a slight decrease in crystallinity. While Na^+ can be used to template the birnessite structure, its performance is apparently not as good as K^+. Additional information relating to the comparison between K^+ and Na^+ as templating cations comes from the interlayer spacing in the birnessite structure. While there are no trends apparent in the data as either the KOH or the NaOH concentration is changed, the average interlayer spacings are 0.721 ± 0.003 nm for K^+ and 0.729 ± 0.003 nm for Na^+. This observation is interesting because K^+ is a larger ion than Na^+ (r_{ion} = 138 and 102 pm, respectively [18]). Clearly there is synergy in the birnessite structure associated with the presence of K^+. Under acidic conditions, as the H_2SO_4 concentration is increased, crystal size is essentially constant (and comparable with that achieved when basic electrolytes are used)

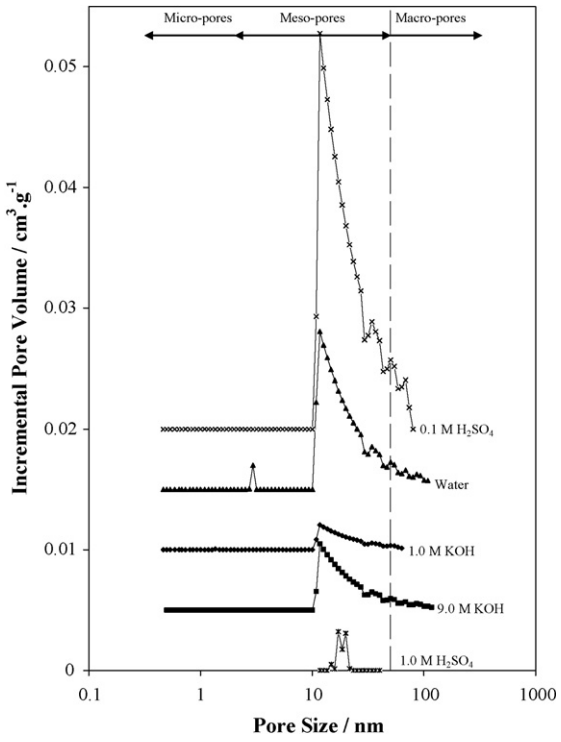

Fig. 6. Pore-size distribution for selected manganese dioxide samples.

for the birnessite samples produced. For comparison with the basic electrolytes, the interlayer spacing for the birnessite samples produced in an acidic environment was 0.724 ± 0.003 nm, which could potentially be influenced by the presence of SO_4^{2-}. As the critical $n(M^+):n(H^+)$ ratio is approached, crystallinity falls slightly and a structural transition is observed. Once β-MnO_2 is established as the preferred phase, crystal size increases dramatically, perhaps reflecting the thermodynamic stability of this phase [19].

3.3. Morphology and porosity

Selected SEM images for the various manganese dioxide samples are presented in Fig. 5(a)–(f). Comparing the images, which cover samples from strong basic to strong acidic electrolytes, reveals a wide variety of morphologies, even for the same crystal structure. Under very basic conditions, such as in 1 M KOH (Fig. 5(a)), the sample appears to consist of platelets of materials that are somewhat agglomerated to form larger particles. In 0.1 M KOH (Fig. 5(b)), while the material structure is still birnessite, sample morphology consists of nanostructured wires tangled together loosely to form an agglomerate, which is combined with a limited number of smaller platelets. With pure water as the solvent (Fig. 5(c)), the morphology is again mixed, with the image dominated by agglomerates of nanowires and what appear to be sheets of manganese dioxide folded together to form porous spherical balls. This latter morphology also predominates when 0.01 M H_2SO_4 is used (Fig. 5(d)). It appears this form grows from a central nucleation site, evidence of which is taken from the apparently early-stage 'split' spherical agglomerates in Fig. 5(c). With 0.1 M H_2SO_4 electrolyte (Fig. 5(e)), the morphology changes again and is now dominated by small platelets. To this point, all of the samples have the birnessite structure, the morphology of which is clearly strongly influenced by solution composition (*v.s.*). With 1 M H_2SO_4, β-MnO_2 is the phase produced. Its morphology is quite different to that of the other samples (Fig. 5(f)), *i.e.*, it takes the form as much larger (note the scale in Fig. 5(f)) inter-grown columns of manganese dioxide.

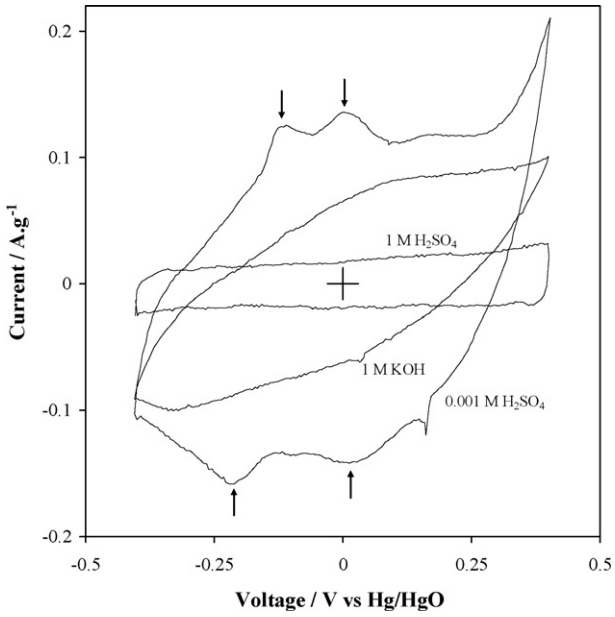

Fig. 7. Examples of voltammetric data collected (scan rate: 5 mV s^{-1} in 9 M KOH electrolyte).

For a material to perform well in a supercapacitor electrode, it must possess not only appreciable porosity, but also a pore-size distribution that allows fast access of diffusing ions to all parts of the electrode. This ensures that capacitance is maintained at high current density. A selection of pore-size distributions is shown in Fig. 6. All materials are essentially meso-porous in nature (dimensions in the range 2–50 nm), with a maximum in incremental pore volume at ~11.5 nm that tapers off towards larger pore dimensions for samples with the birnessite structure. The manganese dioxide sample produced with 1 M H_2SO_4 is also meso-porous. Its pore-size distribution is, however, quite different to that of birnessite samples and thereby suggests that its assemblage of crystallites is also different, as is apparent in Fig. 5. With these materials all being essentially meso-porous in nature, it is expected that their electrochemical performance should display the characteristics of good electrolyte movement during charge–discharge cycling.

3.4. Electrochemical performance

Some typical examples of the electrochemical behaviour of the above materials are collected in Fig. 7. The cyclic voltammograms obtained in 1 M KOH and 0.001 M H_2SO_4 are typical of data collected on the birnessite phase in that they exhibit contributions to the total capacitance from both non-faradaic and faradaic processes. Particularly for the sample prepared in 0.001 M H_2SO_4, the highlighted peaks in the voltammogram are indicative of faradaic processes. By contrast, the sample prepared in 1 M H_2SO_4 (β-MnO_2) exhibits classic capacitive behaviour, and therefore suggests that the faradaic charge-transfer processes for this phase are too sluggish to contribute to the overall capacitance.

Another general feature of the voltammograms is the varying degrees of departure from the rectangular shape that is the expected response for supercapacitor electrodes under these conditions. Typically, curved distortion of the classic 'box' shape is due to the effects of electrode series resistance. There are a number of recent published studies in which the capacitance of thin films of manganese dioxide (<10 μm) have been reported [20]. The advantages of thin films include a lower series resistance due to shorter transport paths, and greater access of the electrolyte to the active surface of manganese dioxide. A major disadvantage, however, is

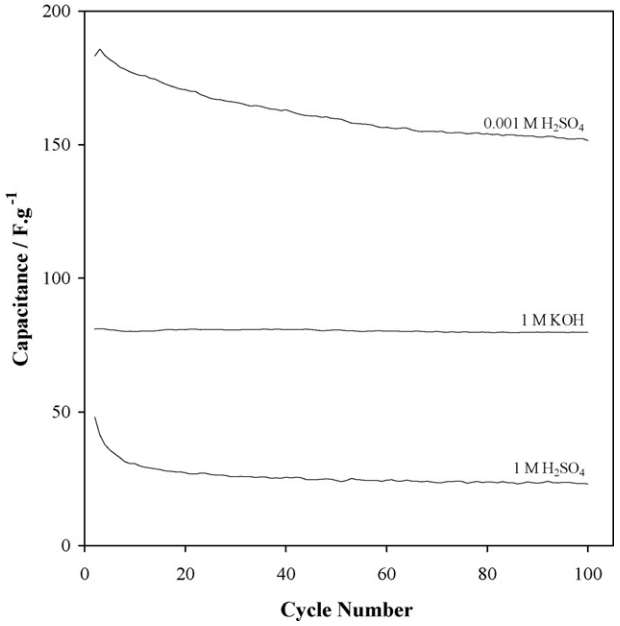

Fig. 8. Cycleability of selected manganese dioxide electrodes (5 mV s^{-1} in 9 M KOH electrolyte).

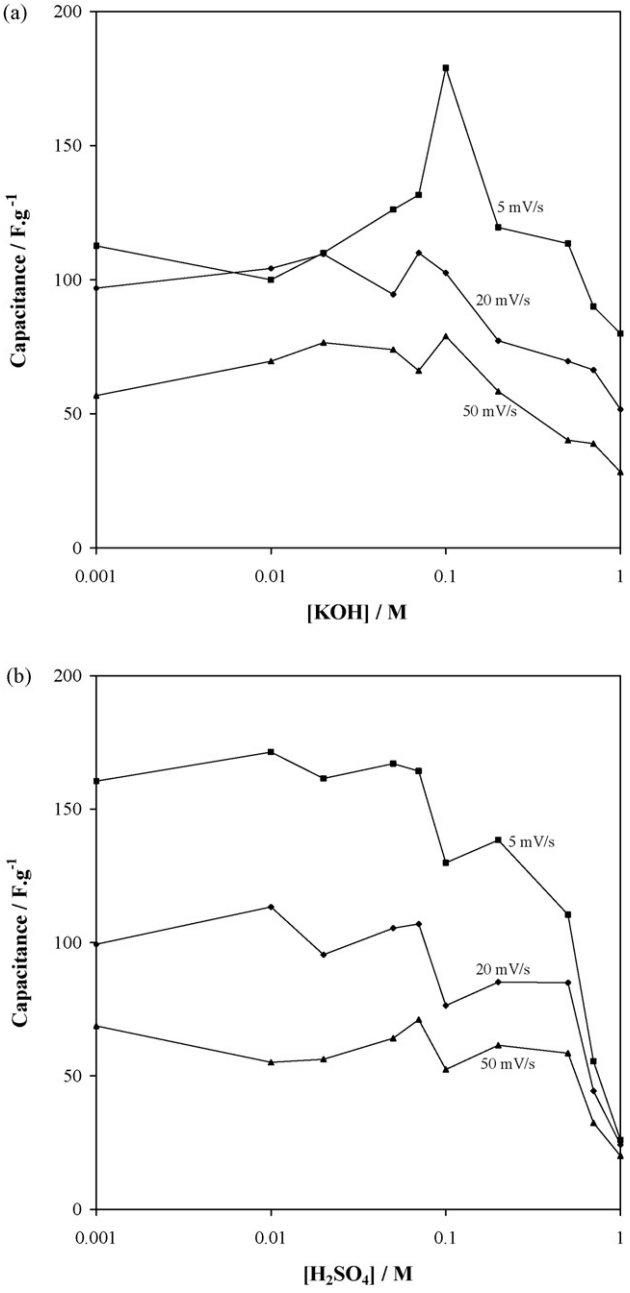

Fig. 9. Performance summary for manganese dioxide samples produced in (a) basic electrolytes, and (b) acidic electrolytes. Specific capacitances reported are plateau values after extended cycling, and after capacitance fade has diminished.

in the preparation and processing, which can be complex. For the relatively thick electrodes used here (~150 μm), series resistance is apparently an issue. This is somewhat compounded by the use of the birnessite phase of manganese dioxide which has a relatively low intrinsic conductivity [21] despite the use of an excess of graphite conductor in the electrode. The only exception is for the sample prepared in 1 M H_2SO_4 (β-MnO_2) that apparently does not suffer from series resistance. This is probably because β-MnO_2 is the most conductive form of manganese dioxide [22], which does suggest that good mixing of the manganese dioxide and conductive material is essential for minimizing series resistance and maximizing performance.

Fig. 8 presents plots of specific capacitance against cycle-number for selected electrode materials, specifically those corresponding to the voltammograms presented in Fig. 7. When birnessite is the dominant phase, and is present in the open nanostructured form that dominates under intermediate-pH preparative conditions, the electrode exhibits considerable loss of capacitance with cycle-life (uppermost trace in Fig. 8). Eventually, the capacitance appears to approach a plateau after extended cycling. By comparison, birnessite produced under strong base conditions, adopts a more dense morphology (Fig. 5(a)), and exhibits essentially constant capacitance (see middle trace in Fig. 8). For the manganese dioxide sample obtained in 1 M H_2SO_4 (β-MnO_2) there is some fade in capacitance, after which a plateau value (20–25 F g^{-1}) is reached. It remains unclear whether the portion of capacitance that is lost is associated with a faradaic or a non-faradaic process or, as apparent here, with both. In general, faradaic processes are more likely to be associated with irreversible loss of storage capacity [23].

In terms of overall material performance, the specific capacitance from each electrode as a function of the electrolyte used for synthesis and the cycling rate is compared in Fig. 9. Note that the capacitance data are the plateau values, recorded after extended cycling. While reports have been published of manganese oxides giving up to 800 F g^{-1}, figures between 100 and 200 F g^{-1} are typically achieved over an extended number of cycles [5]. For relatively thick electrodes, the values obtained in this study (*i.e.*, ~150 F g^{-1} at 5 mV s^{-1}) are therefore commensurate with expectation. The data also suggest that milder electrolytes (intermediate values of pH) give materials with better performance, in particular 0.01–0.10 M KOH and 0.001–0.1 M H_2SO_4. The reason for this behaviour extends back to the effect of electrolyte composition on material crystallinity and porosity. With reference to the XRD data (Fig. 2), the better performing materials have a lower degree of crystallinity (25–50 nm for KOH electrolytes, and 45–60 nm for H_2SO_4 electrolytes). Furthermore, they also possess a larger pore volume, albeit associated with meso-pores. A contrary observation is that, within the whole group of mild electrolytes, larger capacitances are obtained from electrodes made in dilute H_2SO_4 solutions, even though these materials form with larger crystallite size. Here it is assumed that the actual growth and arrangement of crystallites is modified by the choice of electrolyte, thereby leading to greater porosity.

4. Summary and conclusions

A series of manganese dioxide samples has been prepared via the hydrothermal decomposition of permanganate in various electrolytes. The key findings from this investigation are as follows.

(i) The decomposition of MnO_4^- to form manganese dioxide does not occur at an appreciable rate, except at the highest of temperatures examined (200 °C).
(ii) Birnessite manganese dioxide is formed under all conditions, except in electrolytes with >0.5 M H_2SO_4.
(iii) Both K^+ and Na^+ ions template the formation of layered birnessite, and the densest tunnel structures only nucleate when the mole ratio of foreign cations to protons ($n(M^+)$:$n(H^+)$) exceeds unity. Furthermore, the crystallinity tends to increase as the electrolyte concentration is increased, irrespective of whether basic (K^+) or acidic electrolytes are used. Na^+ is not as good a template as K^+; an increase in NaOH concentration causes a decrease in crystallinity.
(iv) The birnessite phase adopts a range of different material morphologies, that include platelets, nano-wires, and spheres.
(v) The materials examined are essentially all meso-porous due to a relatively high degree of crystallization.
(vi) Reasonable electrochemical performance can be achieved from the best electrodes ($\sim$150 F g^{-1} at 5 mV s^{-1} in 9 M KOH) despite the use of relatively thick electrodes and meso-porous materials [5]. The birnessite phase of manganese dioxide derives its capacitance from both a non-faradaic and a faradaic process. The latter process is postulated to be the cause of capacitance fade.

Acknowledgements

The authors acknowledge the contributions made by Dave Phelan and Jenny Zobec from the University of Newcastle Electron Microscopy-X-Ray Facility. BCJ would also like to acknowledge the receipt of a joint CSIRO-University of Newcastle Postgraduate Scholarship.

References

[1] N.S. Lewis, Plenary Lecture 208th Meeting of the Electrochemical Society, Los Angeles CA USA, October, 2005.
[2] D. Ragone, Proc. Soc. Automotive Engineers Conference, Detroit MI USA, May, 1968.
[3] P. Simon, Y. Gogotsi, Nat. Mater. 7 (11) (2008) 845.
[4] B.E. Conway, Electrochemical Supercapacitors: Scientific Fundamentals and Technological Applications, Kluwer-Plenum Publishing Company, New York, 1999.
[5] K. Naoi, P. Simon, Interface 17 (1) (2008) 34 (and references cited therein).
[6] D. Bélanger, T. Brousse, J.W. Long, Interface 17 (1) (2008) 49.
[7] For example: W. Feitknecht, W. Marti, Helv. Chim. Acta 28 (1945) 129; W. Feitknecht, W. Marti, Helv. Chim. Acta 28 (1945) 149; O. Glemser, G. Gattow, H. Meisiek, Z. Anorg. Allg. Chem. 309 (1961) 1; Y.F. Yao, H.S. Wroblowa, J. Electroanal. Chem. 223 (1987) 107; R.M. McKenzie, Miner. Mag. 38 (1971) 493; J.B. Fernandes, B.D. Desai, V.N. Kamat Dalal, J. Power Sources 15 (1985) 209; E. Narita, T. Okabe, Bull. Chem. Soc. Japan 53 (1980) 525; M.H. Rossouw, D.C. Liles, M.M. Thackeray, Prog. Batteries Battery Mater. 15 (1996) 8.
[8] J.W. Long, R.M. Stroud, D.R. Rolison, J. Non-cryst. Solids 285 (1–3) (2001) 288.
[9] CRC Handbook of Chemistry and Physics, D.R. Lide (Ed.), CRC Press, Boca Raton, 1991.
[10] S. Brunauer, P.H. Emmett, E. Teller, J. Am. Chem. Soc. 60 (1938) 309.
[11] P.A. Webb, C. Orr, Analytical Methods in Fine Particle Technology, Micromeritics Corporation, 1997.
[12] V.M. Burns, R.G. Burns, W.K. Zwicker, Proceedings of the Manganese Dioxide Symposium, Cleveland, OH, A.Kozawa and R.J. Brodd (Eds.), I.C. Sample Office and Electrochemical Society, Cleveland (1975) p. 288.; ibid. p. 306.; R.G. Burns, V.M. Burns, Proceedings of the Manganese Dioxide Symposium, Tokyo, B. Schumm Jr., H.M. Joseph and A.Kozawa (Eds.), I.C. Sample Office and Electrochemical Society, Cleveland (1980) p. 97.
[13] W. Buser, P. Graf, W. Feitknecht, Helv. Chim. Acta 27 (1954) 2322.
[14] R. Giovanoli, E. Stähli, W. Feitknecht, Helv. Chim. Acta 53 (1970) 453.
[15] R. Giovanoli, E. Stähli, W. Feitknecht, Helv. Chim. Acta 53 (1970) 209.
[16] J.E. Post, D.R. Veblen, Am. Miner. 75 (1990) 477.
[17] A.R. West, Solid State Chemistry and its Applications, John Wiley and Sons, 1984.
[18] G. Aylward, T. Findlay, SI Chemical Data, sixth ed., John Wiley and Sons, 2008.
[19] M. Pourbaix, Atlas of Electrochemical Equilibria in Aqueous Solutions, Pergamon Press, London, 1966.
[20] (For example) S.C. Pang, M.A. Anderson, T.W. Chapman, J. Electrochem. Soc. 147 (2) (2000) 444.
[21] S.W. Donne, High Performance Chemically and Physically Modified Manganese Dioxide, PhD Thesis, University of Newcastle, Australia, 1996.
[22] K.J. Euler, Metalloberflaeche - Angewandte Elektrochemie 28 (1) (1974) 15.
[23] S.W. Donne, G.A. Lawrance, D.A.J. Swinkels, J. Electrochem. Soc. 144 (9) (1997) 2954.